Open Access

Research Article

PRNANO

Precis. Nanomed. 2024, 7(4):1386-1405

ANDOVER HOUSE

# Synthesis and Characterization of 5-FU-Loaded $CaCO_3$ Nanoparticles for Targeted Cancer Therapy

Kshidan Marim Abdullah Salem[1], Mohamed Ahmed Ibrahim[1,2], Kim Wei Chan[1], Md Zuki Abu Bakar[1,3], Noorjahan Banu Alitheen[4], Mohammed Alsubbi[5], Ahmad Faizal Abdull Razis [1,6,7*] Norsharina Ismail[1**]

[1]*Natural Medicines and Products Research Laboratory, Institute of Bioscience, Universiti Putra Malaysia, Serdang, Selangor Darul Ehsan, Malaysia*

[2]*Department of Pharmaceutics and Industrial Pharmacy, Faculty of Pharmacy, October University for Modern Sciences and Arts (MSA), 12451 Giza, Egypt*

[3]*Department of Veterinary Preclinical Sciences, Faculty of Veterinary Medicine, Universiti Putra Malaysia, Serdang, Selangor Darul Ehsan, Malaysia*

[4]*Department of Cell and Molecular Biology, Faculty of Biotechnology and Biomolecular Sciences, Universiti Putra Malaysia, Serdang, Selangor Darul Ehsan, Malaysia*

[5]*Faculty of Medicine, Sebha University, Sebha, Libya*

[6]*Department of Food Science, Faculty of Food Science and Technology, Universiti Putra Malaysia, Serdang, Selangor Darul Ehsan, Malaysia*

[7]*Laboratory of Food Security and Food Integrity (FOSFI), Institute of Tropical Agriculture and Food Security, Universiti Putra Malaysia, Serdang, Selangor Darul Ehsan, Malaysia*

Submitted: August 17, 2024 Accepted: November 22, 2024 Published: December 22, 2024

## Graphical Abstract

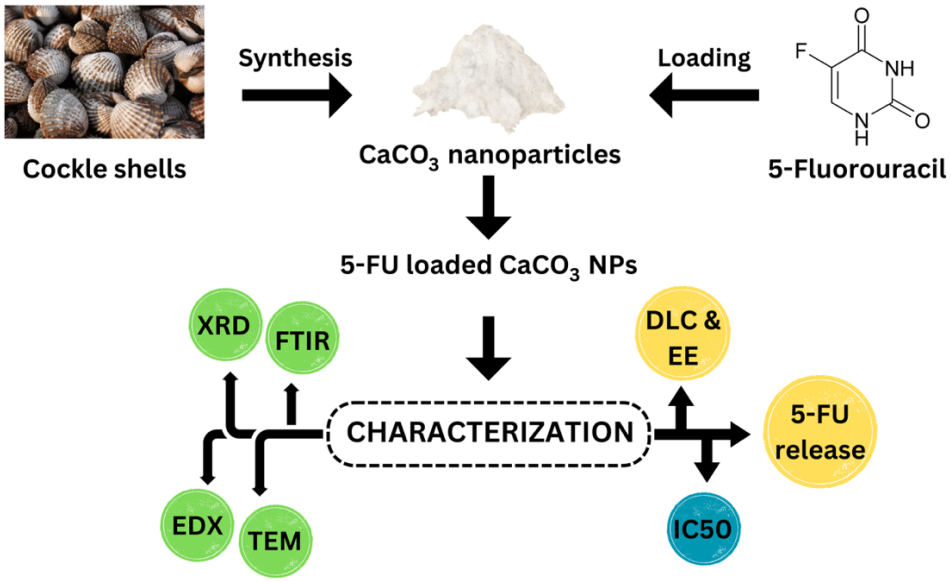


## Abstract

Chemotherapy is often limited by its systemic toxicity and lack of specificity, necessitating the development of targeted drug delivery systems that can enhance therapeutic efficacy while minimizing adverse effects. Addressing this, our study aimed to synthesize and characterize 5-Fluorouracil loaded calcium carbonate nanoparticles derived from cockle shells. The research aimed at increasing site-specific drug release and reducing cytotoxicity. The nanoparticles were prepared using a simple co-precip-

*Correspondence to: madfaizal@upm.edu.my and norsharina@upm.edu.my

itation method, ensuring eco-friendliness and cost-effectiveness. The encapsulation of 5-FU was confirmed by transmission electron microscopy (TEM), which revealed an increase in nanoparticle size from 19.2 ± 2.284 nm for the unloaded ones to 34.8 ± 4.066 nm for the 5-FU-loaded CaCO3 NPs. In vitro release studies demonstrated a pH-sensitive release profile, with more rapid drug release at pH 4.8 compared to pH 7.3. Biocompatibility assays on the HS-27 human skin fibroblast cell line indicated high cell viability, with over 90% maintained even at high nanoparticle concentrations (1000 µg/mL). In addition, cytotoxicity assays on the SW480 (primary colon cancer) and SW620 (metastatic colon cancer) cell lines showed a dose-dependent decrease in cell viability and demonstrated a more controlled and sustained release compared to free 5-FU, resulting in higher cell viability at all time points and concentra-tions. The 5-FU-loaded CaCO3 NPs significantly reduced the immediate cytotoxic effects observed with free 5-FU while effectively targeting cancer cells. These findings suggest that the 5-FU-CaCO3 NPs offer a promising alternative to conventional chemotherapy, providing targeted drug delivery with the potential for reduced systemic toxicity and enhanced therapeutic efficacy.

Keywords: Biocompatibility; Calcium Carbonate Nanoparticles; Chemotherapy; pH-sensitive Release; Targeted Drug Delivery

## Rationale, Purpose, and Limitations

This study was motivated by the critical need to develop more targeted cancer therapies that reduce the systemic toxicity associated with conventional chemotherapy. The purpose was to synthesize and characterize biogenic $CaCO_3$ nanoparticles loaded with 5-FU, aiming to improve the therapeutic index of 5-FU through targeted delivery. This research seeks to advance nanotechnology applications by providing a potentially safer, more effective drug delivery method. However, the limitations include the lack of in vivo studies, which may affect the translatability of the findings.

## Introduction

Nanotechnology has seen a significant surge in its application in the medical field, particularly in biomedical applications such as molecular imaging diagnosis, tissue engineering, and targeted drug delivery. This has led to a great increase in the use of nanoparticles for these purposes [1][2][3]. In clinical practice, nanotechnology improves pharmaceuticals' therapeutic index and can potentially enable therapeutic modalities [4]. Specifically, inorganic nanocarriers, such as calcium carbonate nanoparticles derived from biogenic cockle shells, have been synthesized to deliver anticancer drugs [5] [6]. These are gaining prominence due to their stability, robustness, and larger surface area for drug binding, enabling them to deliver more drugs than organic nanocarriers. Biosynthesized or biogenic nanoparticles, such as those from cockle shell-derived calcium carbonate ($CaCO_3$), demonstrate promising potential as efficient drug delivery systems. They have shown prospects as nano-sized drug carriers specifically targeting cancer cells [8][10]. This is particularly evident in the use of $CaCO_3$-doxorubicin nanoparticles, which have exhibited higher toxic effects on cancer cells compared to doxorubicin alone, highlighting the effectiveness of the doxorubicin/nanocrystals approach in cancer therapy [11][12]. The versatility of nanomaterials extends to their application in therapeutic agents, diagnostic imaging systems, and drug delivery systems. Nanomaterials also serve as imaging agents/contrasts for monitoring the disease status in vivo using various imaging modalities [13]. In cancer therapy, nanoparticles offer specific advantages such as biocompatibility, reduced toxicity, greater stability, enhanced permeability and retention effect, and precise targeting. They have been modified for a wide range of cancer therapies to target cancer cells, the tumor microenvironment, and the immune system, thus overcoming toxicity and lack of specificity enhancing drug capacity and bioavailability [14].

Using inorganic biobased material like aragonite polymorph in drug delivery offers significant advantages over assembled organic polymers due to its biocompatibility, biodegradability, and stimuli responsiveness, which enhances selectivity against specific cells [15] [16]. The structural surface porosity of the cockle shell-$CaCO_3$ nanomaterial facilitates the incorporation of both water-soluble and insoluble anticancer drugs, thus improving the loading capacity of the nanocarrier Additionally, upon decomposition, calcium ions are utilized for various biochemical activities, including cell proliferation, tissue contractile, hemopoietic regulation, and inducing

apoptotic cell death through increased cytoplasmic calcium influx, with carbon dioxide being liberated through gaseous exchange [19] [20]. This has led to the continuous development of new nanocarriers to improve the therapeutic index of conventional anticancer agents using biogenic inorganic nanomaterial [21]. Previous studies have extensively studied the naturally incorporated alginate enclosed, calcium carbon, and chitosan phosphate nanoparticles for microbial infections (AEC-CCO-CP-NP) [22] [23].

Fluorouracil (5-FU) is a widely used chemotherapeutic agent for various neoplasms and as a palliative treatment for advanced gastrointestinal cancers. It is a prodrug converted to active metabolites responsible for its therapeutic effects. The synthesis of homogeneous $CaCO_3$ nanoparticles ($CaCO_3$ - NPs) with high loading content and encapsulation efficiency is desirable for the controlled and sustained release of its conjugated therapeutic agents at specific sites for pharmacological action). The $CaCO_3$ nanoparticle synthesis using the mechanical stirring technique in the presence of dodecyl dimethyl betaine (BS-12) demonstrated high homogeneity of sample product with good nanoparticle dispersion, and it showed pH-sensitive nanocarrier for effective delivery of doxorubicin on MCF-7 breast cancer cell line [24]. Considering these advancements, this experiment aimed to synthesize and characterize homogeneous aragonite $CaCO_3$ NP conjugated with 5-FU, determine the loading content, improve the therapeutic index of 5-FU, and determine the cytotoxicity of this drug. This focus on $CaCO_3$ and 5-FU nanocomposites is a testament to the emerging nanotechnology applications in the medical field.

## Materials and Methods

### Materials

The human skin fibroblast cell line (HS-27) and colon cancer cell lines (SW480 and SW620) were obtained from the American Type Culture Collection (ATCC, USA). Dodecyl dimethyl betaine (BS-12) was purchased from Jindun Chemical (China), while 5-fluorouracil (5-FU), fetal bovine serum (FBS), and the antibiotic solution (penicillin-streptomycin) were supplied by Sigma-Aldrich (USA). Dulbecco's Modified Eagle Medium/Nutrient Mixture F-12 (DMEM-F12), Roswell Park Memorial Institute (RPMI) medium, phosphate-buffered saline (PBS), and trypsin-EDTA solution were acquired from Gibco (USA). 3-(4,5-dimethylthiazol-2-yl)-2,5-diphenyltetrazolium bromide (MTT) reagent was obtained from Nacalai Tesque (Japan).

### Methods

#### *Preparation of Cockle Shells-derived Calcium Carbonate Nanoparticles ($CaCO_3$ NPs)*

Nanoparticles of calcium carbonate were prepared from cockle shells according to the previously described by [25] [26] with some modifications. The cockle shells were cleaned, boiled, and dried in the oven at 50°C for 14 days. The shells were ground using a blender (RPM 25,000 ~ 30,000 RPM) and then sieved using a 90 µm stainless steel laboratory sieve followed by a 75 µm to obtain a micro-sized powder. 50 ml of deionized water was mixed with 5g of micronized powder and then placed on a magnetic stirrer for 30 minutes at 1000 rpm. While placing the conical flask in a sonicator for 5 minutes, the $CaCO_3$ was then synthesized by adding 0.5 mL of Dodecyl dimethyl betaine (BS-12) (Jindun Chemical, China) into the mixture and stirred vigorously at 1,000 rpm for 2 hours at 25°C. Subsequently, the BS-12 was removed by a high-speed centrifuge (10000 rpm/15000 xg, 10 min, 24-25°C) and dried in an oven for two days. The dried nanoparticles were then placed in a 250 mL medium-sized jar containing ceramic balls (9 medium marbles and seven small marbles) and rolled on the ball miller at 200 rpm for 850 hours while placed on a Systematic Multi-Hotplate stirring machine (Systematic Multi-Hotplate Stirrers 6 Positions, WiseStir® Korea). The fine CaCO3 nanoparticle was then packaged and stored in the oven at 50°C until it was used.

#### *Morphology and Elemental Analysis*

The size and shape of the samples were evaluated using TEM (HitachiH-7100, Japan) operated at a voltage of 150 kV. The sample was first mixed with absolute alcohol and sonicated using a Sonicator (Power Sonic 505, South Korea) for 30 min. A drop of the colloidal solution was then placed onto a carbon-covered copper grid on a piece of filter paper and dried at room temperature for an hour. The elemental compassion of the sample was examined using a Field Emission Scanning Electron Microscopy

equipped with an energy-dispersive X-ray spectroscopy (EDX) unit (FESEM, JOEL 7600F, Japan) operated at a voltage of 5kV. All samples were dispersed onto carbon conductive adhesive, placed on the sample holder, and then coated with platinum before being examined under the electron microscope.

### *Zeta Potential and Polydispersity Index (PDI)*

The surface charge and PDI of the nanoparticles were measured using a Zeta Sizer Nano ZS (Malvern Instruments Ltd. Version 7.02, UK). Samples of both plain $CaCO_3$-NP and 5-FU-loaded $CaCO_3$NP were prepared by dissolving in a 1:1 mixture of deionized water and ethanol, followed by 30 minutes of sonication. The solutions were then transferred to cuvettes for analysis. All the measurements were made in triplicates at a temperature of 25°C. The polydispersity index (PDI) values will be averaged and expressed as mean ± standard deviation of three replicate measurements.

### *Fourier Transform Infrared Spectroscopy (FTIR)*

FTIR spectroscopy (Model 100 series, Bruker Invenio R, Germany) was used to analyze the chemical properties of the samples, and the absorption spectra were 400 – 4000 $cm^{-1}$ at a motion of 4 $cm^{-1}$ and a speed of 32 scans per second [27].

### *X-ray Powder Diffraction (XRD)*

The purity and crystalline properties of samples were examined using a Shimadzu XRD (Model; 6000, Japan). Traverse sections of the specimen were placed on a quartz plate for exposure to Cu Kα radiation wavelength of λ=1.5406 Ã. The samples were scanned at diffraction angles from 2° to 80° to obtain unique patterns of reflection peaks at different angles and intensities at room temperature, over 2Ɵ ranges of 20–60°, and at sampling intervals 2θ=0.02° at a scanning rate of 0.6°/min [27].

### *Evaluation of 5-FU Drug-Loading Capacity (DLC) and Encapsulation Efficiency (EE) of $CaCO_3$ NPs*

The quantification of the concentration of 5-FU entrapped by the $CaCO_3$ NPs is essential in the drug delivery system. Thus, it is fundamental to determine the amount of drug entrapped per the ratio of the carrier used with some notifications [18]. A standard calibration curve was generated using the absorbance at 265 nm to quantify 5-FU concentrations. For this, known concentrations of 5-FU were prepared in a solvent mixture of deionized water and isopropanol. The calibration curve was then used to calculate the amount of 5-FU encapsulated in the $CaCO_3$ NPs by determining the 5-FU concentration in the supernatant, representing the un-encapsulated drug.

Based on preliminary optimization, six experimental formulations were prepared, combining $CaCO_3$ NPs with five different concentrations of 5-FU (6, 9, 15, 18, and 21 mg). Each formulation consisted of 30 mg of $CaCO_3$ NPs loaded with 5-FU, dissolved in 5 mL of ddH2O, and stirred overnight at 200 rpm in a dark room. Separation of the un-entrapped 5-FU from $CaCO_3$ NPs was achieved by ultracentrifugation at 15,000 xg for 10 min at 27°C (Hitachi Koki Co., Ltd., Japan).

$$\text{Drug} - \text{loading Content (DLC \%)} = \frac{\text{Mass of drug loaded to the NP (mg)}}{\text{Mass Total (mg)}} \times 100\%$$

$$\text{Encapsulation Efficiency (EE \%)} = \frac{\text{mass of drug loaded to the NP (mg)}}{\text{Initial mass of drug used to the NP (mg)}} \times 100\%$$

The sediment of loaded conjugates was washed with deionized water twice and freeze-dried. The drug-loading content and encapsulation efficiency of the $CaCO_3$ NPs were analyzed by calculating the difference between the total amount of the 5-FU feed and the un-trapped 5-FU concentration in the supernatant of the suspension per weight of $CaCO_3$ NPs. The concentrations of the free 5-FU in the supernatant aliquot were determined by measuring the absorbance 265 nM for 5-FU with a UV spectrophotometer (UV-1650PC-Shimadzu, Japan).

Data for DLC %) and encapsulation efficiency (EE %) of $CaCO_3$NP were obtained from three independent measurements, calculated using Equations 1 and 2 [28]

### *In vitro Drug Release Study*

The in vitro release of 5-FU in free form and from selected prepared $CaCO_3$ NPs was evaluated employing the dialysis bag technique (molecular weight cut-off 12.000–14.000 Da) [29]. An amount equivalent to 3 mg of 5-FU was instilled in the dialysis bag, sealed at both ends to prevent leakage, and placed in screw-capped glass containers filled with 100 mL PBS (pH 4.8 and 7.3) and PBS containing 0.02% Tween 80. The mechanism for drug release in aqueous media is drug diffusion. 5-FU, a hydrophilic drug, and tween 80 were added in PBS to increase its solubility and thus aid in releasing 5-FU. The system was kept at 37°C at 100 rpm using a heating magnetic stirrer (Systematic Multi-Hotplate Stirrers 6 Positions, WiseStir® Korea). At predetermined time intervals (0, 2, 4, 6, 8, 10, 12, 24, 48, and 72 h), 3 mL of the release medium was withdrawn and replaced with 3 mL of fresh buffer solution. The samples were adequately diluted and analyzed for 5-FU content spectrophotometrically at 265 nm. The cumulative percentage of drug released was determined as the ratio of the amount of released 5-FU to the amount of 5-FU initially inserted into the dialysis bag. All measurements were performed in triplicates [30][31].

### *Drug Release Kinetics*

To understand the drug release behavior from the developed 5-FU-$CaCO_3$ NPs hollow networks, various in vitro kinetic models were applied, such as zero order, 1st order, Higuchi, Korsmeyer-Peppas, Weibull, Logistic, Gompertz, and Probit [32]. Regression analysis was employed to determine the best-fit model, using the $R^2$ value as a fit measure. The following model equations were used [21].

$$Mt = M0 + k0\ t$$

$$\log Mt = \log M0 + k1\ t$$

$$Mt = kH\sqrt{t}\ M0$$

$$Mt\ 1/3\ M\ t1/3 = Kwt$$

$$Mt1/3 / M\infty\ 1/3 = Kmt\ n$$

Where $M_0$ is the initial amount of 5-FU in dissolution media, $M_t$ is the amount of 5-FU in dissolution media at time t, $k_0$, $k_1$, $k_H$, $k_w$, $k_m$ are dissolution rate constants, $M_t / M_\infty$ is the fraction of 5-FU released at time t. The n is used to characterize different release mechanisms.

Finally, the coefficient of determination ($R^2$) was considered to measure the best-fit model equation, representing the release pattern. The 5-FU released percentage of all nanoparticles was determined as the ratio of the released amount of 5-FU to the total loaded amount of 5-FU.

### *Cell Culture / Biocompatibility Assay*

The SW40 and SW620 cell lines were cultured in RPMI-1640 media, while DMEM F-12 was used for the HS-27 cells, and all media contained 10% FBS and 1% penicillin-streptomycin solution. All cells were grown in a humified incubator at 37◦C and 5% $CO_2$. Cell lines were cultured with different concentrations of 5-FU, blank $CaCO_3$ NPs, or 5-FU-$CaCO_3$ NPs for 24, 48, and 72 hours. Briefly, the cells were seeded ($5\times10^3$ cells/well) in a 96-well plate followed by 24 hours incubation. Then, different concentrations of blank $CaCO_3$ NPs (ranging from 0 to 1000 µg/mL) or 5-FU-$CaCO_3$ NPs (ranging from 0 to 100 µg/mL) were added. After appropriate treatment, 20 µL of MTT solution (5 mg/mL) was added into each well and incubated for 4 hours. The MTT solution was then removed by careful pipetting, and 150 µL DMSO was added per well to dissolve the formazan crystals. After 30 mins, the absorbance of each well was read at 570 nm using a microplate reader (Tecan Infinite, Switzerland) [33].

SW480 and SW620 human colon cancer cell lines were obtained from the American Type Culture Collection (ATCC, USA) Cell Culture Facility. Three independent replicates of SW480 cells were seeded at 40,000 cells/$cm^2$ in a T-175 culture flask, incubated at 37°C and 5% $CO_2$ in RPMI RPMI high glucose (Sigma-Aldrich) supplemented with 10% FBS and 2% ultraglutamine,1% non-essential amino acids (Sigma-Aldrich) and 1% Ultraglutamine (Lonza). Cellular viability was assessed by trypan blue (Sigma-Aldrich) exclusion, and cell

count was performed using a Burker chamber. Cells were incubated at 37°C in a humidified atmosphere of 5% $CO_2$ until they reached about 60–70% confluence. The culture media were then aspirated, and cells were washed three times with 1× Dulbecco's PBS. w/o calcium and magnesium and once with serum-free culture media. Cells were then grown in 10 ml of complete culture medium without serum for 24 h. Thereafter, for each independent experiment, the conditioned media from 15 T-175 flasks were collected for each cellular model system, supplemented with a Complete Mini protease inhibitor cocktail, and centrifuged at 400*g* for 15 min at 4°C. Following the collection of the conditioned media [34] [35].

### *Statistical Analysis*

Data were expressed as mean ± SD and percentage. Analysis was conducted using ImageJ, SPSS version 22, Origin Pro 2024, and GraphPad Prism 9 software. In vitro kinetic model parameters were computed using the DDSolver add-in for Excel. Statistical comparisons between groups were performed using an independent Student's t-test. The level of significance was set at $p < 0.05$.

## Results and Discussion

### Fourier Transform Infrared Spectrophotometer (FTIR) Chemical Analysis

The FTIR spectra of cockle shell-derived $CaCO_3$ NPs, free 5-FU, and 5-FU-loaded $CaCO_3$ NPsare presented to elucidate the structural integrity and interaction between 5-FU and $CaCO_3$ in the formulation of the nanocomposite drug delivery system (Figure 1). The FTIR spectrum of free $CaCO_3$ exhibited characteristic absorption bands at approximately 1420 $cm^{-1}$ and 875 $cm^{-1}$, which can be attributed to the carbonate ions' asymmetric and out-of-plane bending vibrations ($CO_3^{2-}$). The literature corroborates these peaks as indicative of calcium carbonate's aragonite phase, typically seen at 1447, 1082, 854, and 708 $cm^{-1}$ [25] [36] [18]. The slight shift in peaks for the drug-loaded $CaCO_3$ NPs to 1473, 1078, 859, and 761 $cm^{-1}$ suggests the incorporation of 5-FU without altering the structural integrity of the aragonite form. The spectrum of free 5-FU reveals multiple absorption peaks, including those around 1700 $cm^{-1}$ characteristic of the carbonyl (C=O) stretch, and other peaks that correspond to the aromatic ring and fluorine atom vibrations, which are intrinsic to the 5-FU molecular structure. Moreover, 5-FU bears amino ($–NH_2$) functional groups and shows absorption peaks around 3000 $cm^{-1}$ [37].

Upon loading 5-FU onto $CaCO_3$ NPs, notable changes were observed in the FTIR spectrum. The distinctive peaks corresponding to 5-FU appear to diminish or are no longer discernible, suggesting encapsulation within the porous structure of $CaCO_3$ NPs compared to the previous studies [38]. The apparent disappearance of these peaks could indicate the successful loading of 5-FU into the $CaCO_3$ NPs matrix, potentially due to the internalization of the drug within the pores of the nanoparticles. This encapsulation is hypothesized to alter the vibrational energy of the 5-FU functional groups, rendering their signature peaks less pronounced. The interaction between 5-FU and $CaCO_3$ NPs is a critical factor in determining the stability and release profile of the drug from the nanocomposite. The spectrum of the 5-FU-loaded $CaCO_3$ NPs did not show new peaks, which could have implied a chemical interaction or bond formation between the drug and the carrier. Instead, the observed peak attenuation supports a physical encapsulation mechanism, where the drug is entrapped within the $CaCO_3$ NPs matrix without significant chemical modification. This could be advantageous for maintaining the drug's efficacy while enabling a controlled release. These results have significant implications for developing targeted cancer drug delivery systems. The physical encapsulation of 5-FU within $CaCO_3$ NPs has the potential to protect the drug from premature degradation in the physiological environment, thereby enhancing its bioavailability and therapeutic effect. Furthermore, the porous nature of $CaCO_3$ NPs may allow for a sustained release of 5-FU, which is desirable in minimizing the side effects of high systemic drug concentrations [39].

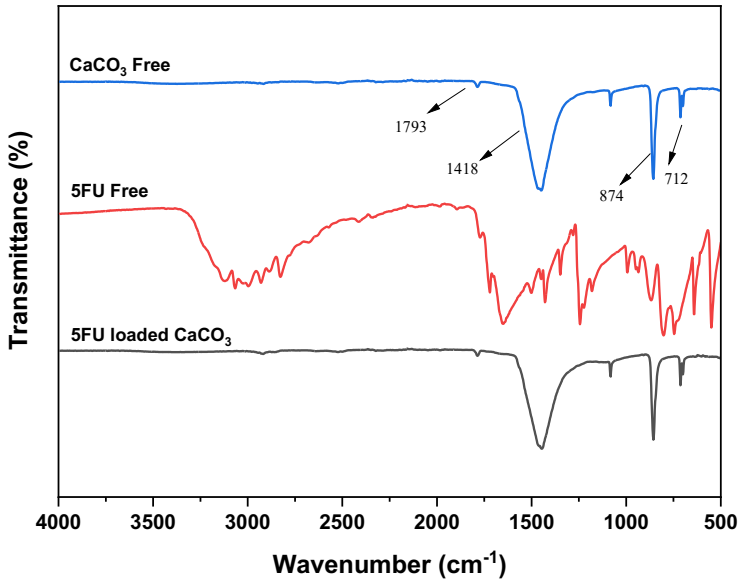


*Figure 1. FT-IR spectra of calcium carbonate nanoparticles (CaCO3 NPs), 5-fluorouracil (5-FU), and 5-FU-loaded CaCO3 NPs.*

## X-Ray Powder Diffraction (XRD)

X-ray diffraction (XRD) analysis was conducted to investigate the structural properties of pure $CaCO_3$ NPs, free 5-FU and 5-FU loaded onto $CaCO_3$ NPs. The resulting XRD patterns (Figure 2) provide insight into the synthesized nanocomposites' crystallinity and potential drug-carrier interactions. Figure 2A displays the XRD pattern of pure $CaCO_3$ NPs, with distinct peaks that confirm the aragonite structure, as corroborated by comparison with the reference diffraction peak from the Joint Committee on Powder Diffraction Standards (JCPDS) file, specifically number 00-041-1475. This match underscores the synthesized nanoparticles' high crystallinity and validates their structural identity as aragonite, which is a crucial aspect of their suitability for drug delivery applications [37] [40].

In Figure 2B, the free 5-FU shows a highly crystalline XRD pattern, with sharp and intense peaks characteristic of the pure drug. The XRD pattern for the 5-FU loaded $CaCO_3$ Nps (Figure 2C) combines the characteristics of both the $CaCO_3$ NPs and 5-FU. Notably, the similarity in the diffraction patterns of the blank $CaCO_3$ NPs and the drug-loaded $CaCO_3$ NPs suggests that the crystallinity of the $CaCO_3$ NPs is retained post-drug-loading. This observation is critical as it suggests that the $CaCO_3$ NPs remain stable through the drug-loading procedure, retaining their structure. This is vital for their performance as a drug delivery system. The changes observed in the crystallinity of 5-FU upon loading into the nanoparticles could be attributed to the intercalation of drug molecules within the $CaCO_3$ lattice, creating a less ordered structure. This disruption can be advantageous, potentially allowing for a more controlled and sustained drug release profile due to the increased interaction between the drug and the carrier [41].

## Energy-Dispersive X-ray (EDX)

The energy-dispersive X-ray (EDX) spectroscopy analysis of 5-FU-$CaCO_3$ NPs, as depicted in the spectral peak data, confirms the primary composition of the cockle shell-derived calcium carbonate aragonite nanoparticles, showcasing prominent peaks for oxygen (O), carbon (C), and calcium (Ca), consistent with the expected constituents of $CaCO_3$. The detected elements' quantitative representation aligns with previous studies [26][42]. The calcium content range is 20.16–23.63%, alongside carbon content at 24.45–26.26%. Notably, the spectrum does not distinctly feature sulfur (S), suggesting its minimal presence or an overlap with other elemental signals.

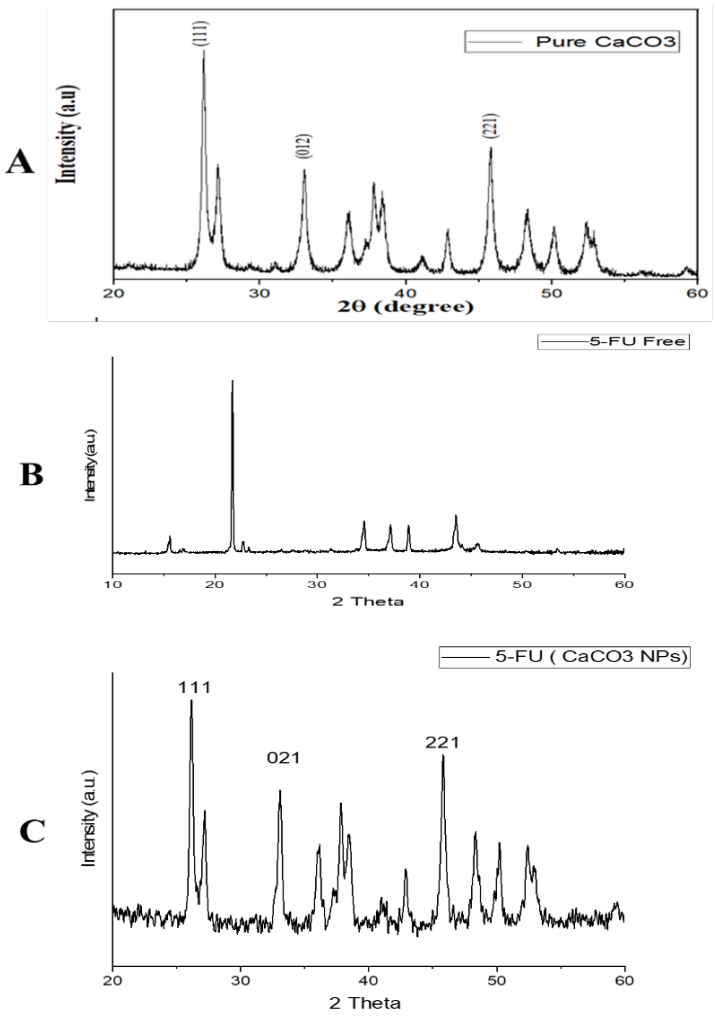


*Figure 2. XRD patterns of (A) pure calcium carbonate nanoparticles (CaCO3 NPs), (B) free 5-Fluorouracil (5-FU), and (C) 5-FU-loaded CaCO3 NPs*

The trace presence of other elements, such as sodium (Na), aluminum (Al), silicon (Si), and platinum (Pt), could be attributed to the synthetic process or sample handling. The results endorse the NPs' compositional integrity and pave the way for discussing the implications of such a composition on the therapeutic efficacy and delivery mechanism of 5-FU [43].

## Size Determination Using TEM

Transmission electron microscopy was employed to ascertain the size and morphology of the nanoparticles before and after the loading of 5-FU. Figure 4 illustrates the TEM images and the corresponding size distribution histograms.

Before drug encapsulation, the cockle shell-derived $CaCO_3$ NPs exhibited a mean diameter of 19.26 ± 2.28 nm. After the loading with 5-FU, a significant increase in size was observed, with the 5-FU-$CaCO_3$ NPs displaying a mean diameter of 34.88 ± 4.06 nm, as seen in (Table 1). The results indicate the successful encapsulation of 5-FU within the $CaCO_3$ NPs, as reflected by the increase in the mean diameter size post-drug loading (Table 1). The size increase from 19.26 nm to 34.88 nm is substantial. It is within the desirable range for nanoparticle-based drug delivery, ensuring a sufficient surface area-to-volume ratio for effective drug release and cellular uptake.

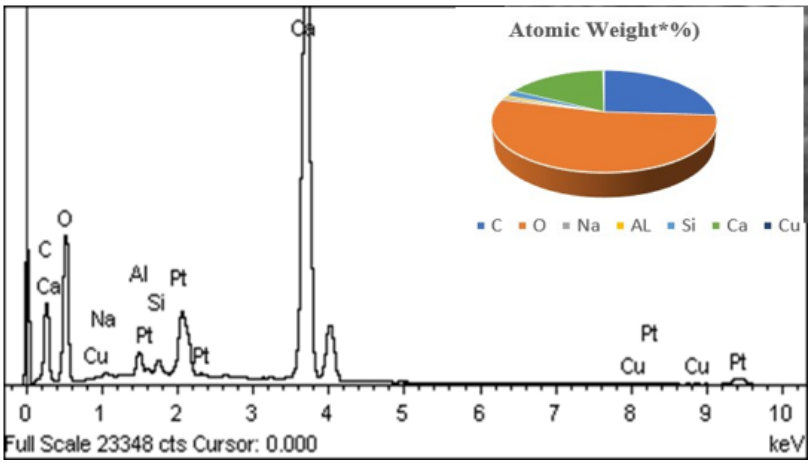


*Figure 3. Spectral peak data of 5-FU-CaCO3 NPs for EDX spectroscopy.*

Moreover, the relatively narrow size distribution post encapsulation (SD = 4.06 nm) suggests a homogeneous population of nanoparticles, which is essential for consistent drug dosing and predictable pharmacokinetics. Previous studies have reported similar patterns.[44] [52] [42] [53] Nanoparticles smaller than 50 nm are likely to be excreted by the kidneys before reaching their target. In comparison, larger sizes greater than 100 nm are more likely to be sequestered by the reticuloendothelial system (RES) [46]. However, a large percentage of free $CaCO_3$ NPs and drug-loaded $CaCO_3$ NPs fall between the two extremes. This intermediate size range is advantageous as it potentially avoids rapid elimination by the kidneys and evasion by the RES, making $CaCO_3$ NPs an excellent choice for targeted drug delivery systems. Their size allows them to circulate longer in the bloodstream, enhancing the likelihood of reaching and accumulating at the target site [47][48].

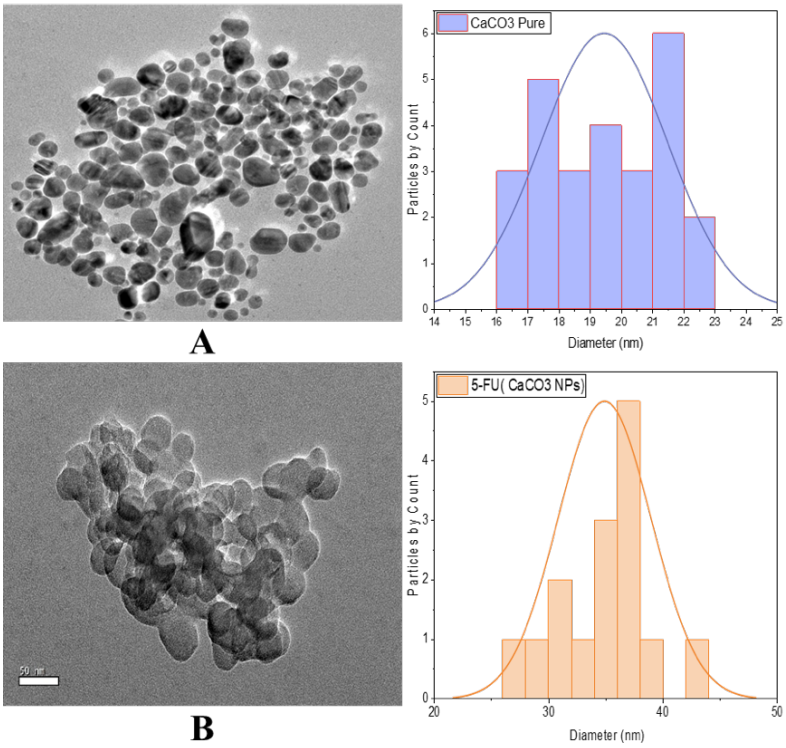


*Figure 4. TEM image of (A) calcium carbonate nanoparticles (CaCO3 NPs) and (B) 5-fluorouracil loaded calcium carbonate nanoparticles (5-FU-CaCO3 NPs) with corresponding size distribution histograms.*

**Table 1. CaCO3 NPs and 5-FU-CaCO3 NPs diameter size.**

| Nanoparticle | Diameter size in mean ± SD (nm) |
|---|---|
| CaCO3 NPs | 19.26 ± 2.28 |
| 5-FU-CaCO3 NPs | 34.88 ± 4.06 |

Results are means ± standard deviation of three determinations.

## DLC and Encapsulation Efficiency (EE)

Notably, $CaCO_3$ NPs can load various drugs regardless of their hydrophobicity or surface charge characteristics. In our experiments, 5-FU was loaded into $CaCO_3$ NPs at different concentrations. As depicted in Table 2, the EE of 5-FU-$CaCO_3$ NPs remained consistently high (>95%) across varying 5-FU concentrations. Such high EE values indicate the compatibility between the drug and the nanoparticle matrix and the effectiveness of loading the drug. Conversely, the DLC exhibited a positive correlation with the amount of drug used during the formulation process. As the weight of the drug increased, the DLC also increased, reaching a maximum of 40%. However, it is noteworthy that the DLC did not increase proportionally with the amount of drug used, indicating a limit to how much drug the nanoparticles can accommodate before reaching a saturation point. The sample with 18 mg of 5-FU exhibited the highest LC (36.29%) and a high EE (96.61%), making it optimal for further studies. These results align with the previous findings that reported similar trends in nanoparticle drug delivery systems [49][50].

These findings are promising for applying $CaCO_3$ NPs in targeted drug delivery, providing a high degree of control over the drug load while ensuring efficient encapsulation. In broader contexts, $CaCO_3$ NPs derived from cockle shells have successfully encapsulated various therapeutics. As reported in the literature, these include cytarabine,[46] doxorubicin, [52] parathyroid hormone, [53] thymoquinone, [18] and vancomycin. [41] This versatility underscores the potential of $CaCO_3$ NPs in delivering both hydrophilic and hydrophobic drugs, reinforcing the significance of our findings in the development of targeted cancer drug delivery systems, as shown in Table 2.

**Table 2. Drug-Loading Capacity (DLC) and Encapsulation Efficiency (EE) of the Calcium Carbonate Nanoparticles ($CaCO_3$ NPs).**

| Sample | Weight of CaCO3 NPs (mg) | Weight of Drug (mg) | DLC (%) | EE (%) |
|---|---|---|---|---|
| 5-FU-CaCO3 NPs | 30 | 21 | 38.15 ± 0.11 | 92.64 ± 0.26 |
| | 30 | 18 | 36.29 ± 0.19 | 96.61 ± 0.45 |
| | 30 | 15 | 30.87 ± 0.12 | 92.60 ± 0.37 |
| | 30 | 9 | 21.74 ± 0.22 | 94.21 ± 0.96 |
| | 30 | 6 | 15.11 ± 0.14 | 90.63 ± 0.82 |

Results are means ± standard deviation of three determinations.

DLC = drug-loading capacity; EE = Encapsulation Efficiency; NP = nanoparticles.

## Zeta Potential

Zeta potential values provide insight into the nanoparticles' surface charge and potential stability in colloidal dispersions. The value of zeta potential for good stability is above ±30 mV. High zeta potential averts aggregation of the particles and improves stability due to electric repulsion.[65] [66] The higher the surface charge, the stronger the repellent forces between nanoparticles, and the less likely they will aggregate. The dispersion's aggregation of nanoparticles is noticed with values between -25 to 25 mV due to interparticle Van Der Waal forces [45]. The pure $CaCO_3$ NPs exhibited a zeta potential of -18.08 mV as shown (Table 3), indicating moderate stability, likely due to negatively charged surface groups [56]. Upon drug loading with 5-FU, the zeta potential decreased to -6.53 mV, suggesting a reduction in surface charge. This could be attributed to the drug's

interaction with the nanoparticle surface, potentially neutralizing some surface charges. The Z-average of the particles also changed significantly upon drug loading. The free $CaCO_3$ NPs had a Z-average of 88.07 nm, while the 5-FU-loaded $CaCO_3$ NPs showed a substantial increase in size to 375.70 nm, indicating that the drug loading may result in aggregation or particle growth. This is further supported by the increase in the polydispersity index (PDI), from 0.18 for the pure nanoparticles to 0.25 for the 5-FU-loaded ones. However, a PDI value below 0.3 is typically considered indicative of a relatively homogeneous nanoparticle size distribution in colloidal systems, which suggests that while there is an increase in heterogeneity compared to the unmodified nanoparticles, the drug-loaded nanoparticles still maintain a degree of uniformity that could be acceptable for drug delivery applications [57].

**Table 3. Zeta Potential, Average Particle Size Distribution by Intensity and Polydispersity Index of $CaCO_3$ NPs, 5-FU-$CaCO_3$ NPs, Performed at 24◦C**

| Compound | Zeta Potential (mV) ± SD | Z-Average (d nm) | PDI |
|---|---|---|---|
| CaCO3 NPs | -18.08 ± 3.60 | 88.07 | 0.18 |
| 5-FU-CaCO3 NPs | -6.53 ± 0.87 | 375.70 | 0.25 |

Results are means ± standard deviation of three determinations.

NP = nanoparticles; PDI = Polydispersity Index; SD = standard deviation.

## pH-sensitive Drug Release

The in vitro drug release profiles of 5-FU loaded onto $CaCO_3$ NPs were studied at two different pH levels: pH 7.3 (physiologically neutral pH) and pH 4.8 (acidic pH, similar to many tumor tissues), which simulate the physiological and tumor microenvironment conditions, respectively. As depicted in Figure 5, the release of 5-FU at pH 4.8 is markedly faster, with over 70% of the drug released over 72 hours. In contrast, the release at pH 7.3 is significantly slower, with only about 20% of the drug released during the same period. This release pattern is consistent with previous studies on pH-sensitive drug delivery systems [46][58]. The faster release at pH 4.8 indicates that the acidic environment promotes the dissolution of the $CaCO_3$ nanoparticles, facilitating the release of the encapsulated drug.

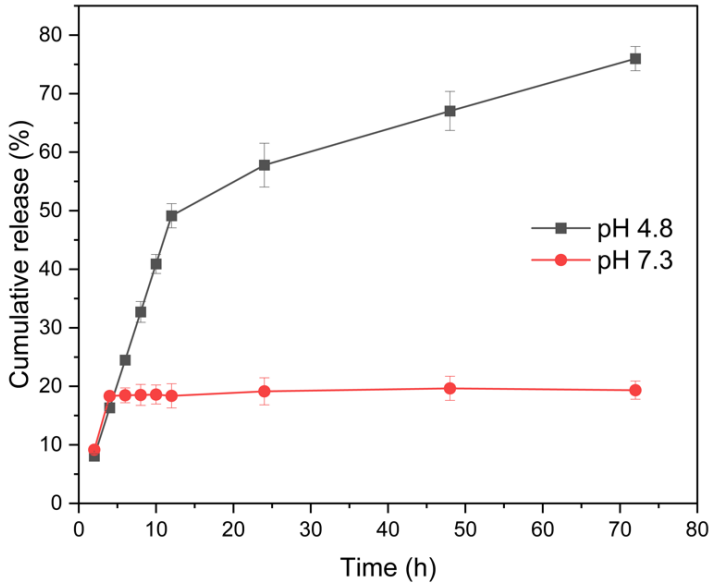


*Figure 5. Release profiles of 5-Fluorouracil (5-FU) from 5-FU loaded calcium carbonate nanoparticles (5-FU- CaCO3 NPs) at pH=7.3 and pH=4.8.*

This release behavior ensures that the drug is rapidly available in acidic tumor environments, where it is needed most. On the other hand, the slower release at pH 7.3 ensures that the drug

remains encapsulated in neutral physiological conditions, minimizing premature release and reducing potential side effects on non-target tissues [65][59]. The addition of Tween 80 in the PBS plays a critical role in enhancing the solubility of 5-FU, which is hydrophilic. This increase in solubility is necessary to facilitate the diffusion of the drug out of the $CaCO_3$ NP matrix, as diffusion is the primary mechanism of drug release in aqueous media. The presence of Tween 80 aids in the solubilization process, ensuring that the drug can be more readily released when the nanoparticles disintegrate in acidic conditions [60][61]].$CaCO_3$ nanoparticles are known to be pH-sensitive, dissolving more rapidly in acidic media (below pH 5) due to the faster degradation of the $CaCO_3$ particles. However, they remain more stable and intact at neutral pH [67][68]. This pH-sensitive release profile underscores the potential of 5-FU-loaded CaCO3 NPs as a targeted drug delivery system. By leveraging the pH differential between normal and tumor tissues, the nanoparticles are engineered to delay drug release until they reach the acidic environment of cancer cells, thus enhancing drug concentration at the tumor site and improving therapeutic efficacy while minimizing effects on healthy tissues [63]. The release profile also demonstrates a sustained release pattern, which is beneficial for maintaining therapeutic drug levels over an extended period. This controlled release could be advantageous in clinical settings, potentially allowing for reduced dosing frequency and improving patient outcomes by delivering the drug more effectively at the target site [69]

## Drug Release Kinetics

To understand the drug release behavior from the developed $CaCO_3$ NPs hollow networks, various in vitro kinetic models were applied, such as zero order, 1st order, Higuchi, Korsmeyer-Peppas, Weibull, Logistic, Gompertz, and Probit. Generally, the $R^2$ value via regression analysis is used to find the best-fit model. The Higuchi model showed the highest coefficients of determination ($R^2$) across drugs at pH 7.3 conditions is 0.9317, while the Korsmeyer-Peppasmodel is 0.9165, indicating that these models are most suited for describing the release kinetics from $CaCO_3$ NPs as shown in (Table 4). By $R^2$ values, Korsmeyer-Peppas is the model that governs the release of 5-FU from the nanoparticles in a neutral solution (pH 7.3). This model was developed in 1983 to describe the release of drug molecules from polymeric matrices [62]. The Higuchi model suggests diffusion-controlled release, while the Korsmeyer-Peppas model indicates a combination of diffusion and erosion mechanisms [52]. This finding has significant implications for applying these nanoparticles in targeted drug delivery. For instance, the sustained release profile indicated by these models is ideal for chemotherapy, where a consistent drug concentration can improve efficacy and minimize side effects [63].

Previous studies have demonstrated varied release kinetics depending on the drug and the nanoparticle composition. For instance, Lee et al. observed that polymeric nanoparticles exhibited a first-order release for hydrophilic drugs [64] in contrast with our findings, where $CaCO_3$ NPs did not fit well with the first-order model for either 5-FU. Moreover, studies on similar $CaCO_3$ NPs loaded with different drugs showed a closer fit to the Hixson-Crowell model, emphasizing the role of surface area and particle size in drug release [58]. However, this model showed a lower $R^2$, especially for 5-FU. It is postulated that additional factors beyond the mere particle size reduction influence the release mechanism from $CaCO_3$ NPs.

## Biocompatibility and Cytotoxicity

### *Biocompatibility Assay of Blank $CaCO_3$ NPs*

The biocompatibility of blank $CaCO_3$ NPs was evaluated on both non-neoplastic human skin fibroblast cells (HS-27) and colon cancer cell lines (SW480 and SW620) using the MTT assay to ensure that the nanocarrier does not exhibit any cytotoxic effects. Figure 6 illustrates that blank $CaCO_3$ NPs had minimal impact on cell viability across all tested cell lines, indicating strong biocompatibility. For HS-27 cells, the viability remained high, decreasing only slightly from 100% at 15.6 µg/mL to 91.72 ± 3.02%. % at 1000 µg/mL after 72 hours of treatment. Similarly, for the SW480 colon cancer cell line, viability dropped from 99.7 ± 0.82% at 15.62 µg/mL to 94.51 ± 3.20% at 1000 µg/mL after 72 hours. The SW620 cell line

showed comparable results, with viability decreasing from 98.87 ± 1.66% at 15.62 µg/mL to 91.31 ± 1.41% at 1000 µg/mL[60]. These results demonstrate that blank $CaCO_3$ NPs are non-toxic across a broad concentration range and do not adversely affect the viability of either non-neoplastic or cancer cells

**Table 4. The Coefficient of Determination ($R^2$) Obtained for 5-FU Release from Nanoparticles in pH 4.8 and 7.3**

| Nanocomposite | Dissolution medium (PBS) | Kinetic model Coefficient of determination (R2) | | | | |
|---|---|---|---|---|---|---|
| | | Zero order | First order | Higuchi | Korsmeyer-peppas | Hixson-Crowell |
| 5-FU-CaCO3 NPs | 4.8 | 0.7001 | 0.3371 | 0.8906 | 0.8742 | 0.8052 |
| | 7.3 | 0.7968 | 0.4712 | 0.9317 | 0.9165 | 0.8634 |

PBS = phosphate-buffered saline.

.

These findings align with previous studies demonstrating the biocompatibility of $CaCO_3$ NPs in various cell types, including MCF10A and MCF cells, [26] [33] UMR-106 rat osteogenic sarcoma cells, MG-63 bone cancer cells, [65] and hFOB 1.19 human fetal osteoblastic cells. [66] Moreover, hybrid alginate/calcium carbonate nanoparticles have been shown to have minimal impact on HeLa cells, [67] further reinforcing the non-cytotoxic nature of $CaCO_3$. As calcium carbonate is a naturally occurring substance in the human body, it contributes to the inherent biocompatibility seen with inorganic nanoparticles [61].

However, cell-type specificity should be considered, as some studies have shown toxicity in particular contexts. For example, one study observed the toxicity of $CaCO_3$ NPs in human endothelial cells (EAhy926) within 24 hours.[68] Interestingly, another study demonstrated that nano-$CaCO_3$ can selectively restrict the aggressiveness of tumor cells (MDA-MB-231) without negatively impacting the surrounding stromal cells, showcasing its potential for selective therapeutic applications [69]. Overall, the biocompatibility of blank $CaCO_3$ NPs suggests they are a promising platform for the safe delivery of therapeutic agents, offering the potential for high-loading capacities without causing harm to healthy or cancerous cells.

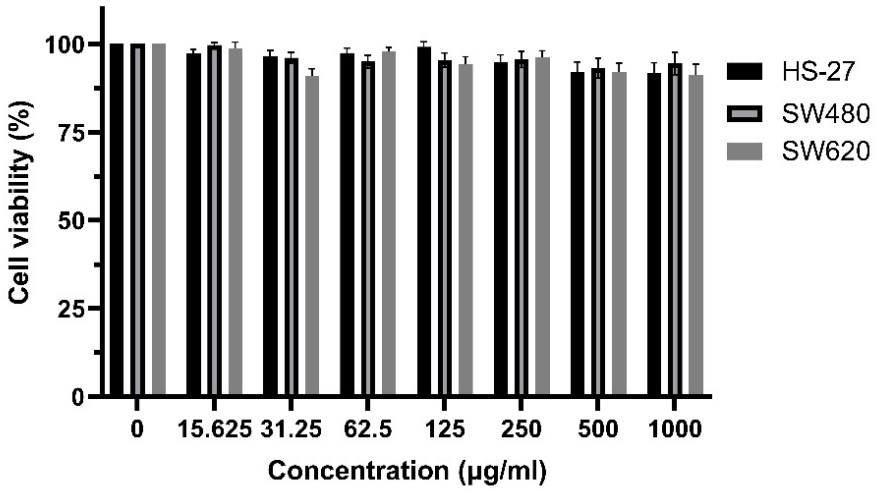


*Figure 6. Biocompatibility of cockle shell-derived calcium carbonate nanoparticles (CaCO3 NPs) on HS-27, SW480, and SW620 after 72 hours incubation.*

## Cytotoxicity of Free 5-FU and 5-FU-loaded CaCO3 Nanoparticles

To evaluate the cytotoxic potential of 5-FU and 5-FU-loaded $CaCO_3$ NPs, cell viability was assessed in non-neoplastic (H-27) and in two colon cancer cell lines, SW480 (primary colon cancer) and SW620 (metastatic colon cancer) over 72 hours. Both formulations, free 5-FU, and 5-FU-loaded $CaCO_3$ NPs, exhibited dose-dependent cytotoxicity but with distinct profiles. Free 5-FU caused rapid cytotoxic effects, whereas the nanoparticle formulation exhibited a more controlled drug release, reducing the immediate cytotoxicity typically observed with free 5-FU. The final concentration of 5-FU used in the nanoparticles was 0.36 mg/mg. For the HS-27 fibroblast cells, treatment with free 5-FU resulted in a prominent decrease in cell viability as the concentration increased. At 3.125 µM, HS-27 cells retained 74.7 ± 0.96% viability, but at the highest concentration of 100 µM, viability dropped to 32.65 ± 0.14%. This significant reduction reflects the inherent cytotoxicity of 5-FU, even in non-cancerous cells. In contrast, 5-FU-loaded $CaCO_3$ NPs demonstrated minimal toxicity, maintaining high cell viability (ranging from 89.26 ± 4.77% to 84.87 ± 6.96% over the same concentration range). These results indicate that $CaCO_3$ nanoparticles act as an effective drug delivery vehicle, providing a more controlled release of 5-FU and significantly reducing its cytotoxic effects on healthy, non-neoplastic cells.

For SW480 cells (Figure 7 A–C), treatment with free 5-FU caused a sharp, dose-dependent decrease in cell viability. After 24 hours, cell viability dropped significantly, from 84.62 ± 4.70% at 3.125 µg/mL to 18.63 ± 5.96% at 100 µg/mL. Conversely, 5-FU-loaded $CaCO_3$ NPs preserved higher cell viability, with 98.88 ± 2.70% viability at 3.125 µg/mL, decreasing to 51.55 ± 3.72% at 100 µg/mL. This pattern persisted at 48 and 72 hours, with the 5-FU-loaded $CaCO_3$ NPs maintaining markedly higher cell viability compared to free 5-FU at all tested concentrations. After 72 hours, free 5-FU reduced cell viability to 28.11 ± 3.20% at the highest dose, while the 5-FU-loaded $CaCO_3$ NPs maintained around 53.18 ± 3.90% viability at the same concentration. This indicates that the $CaCO_3$ nanoparticle system allows for a sustained and controlled release of 5-FU, reducing cytotoxicity compared to free 5-FU while still effectively targeting cancer cells. The sustained drug release from the NPs helps mitigate the sharp cytotoxic effects commonly seen with the free drug.

A similar trend was observed for the SW620 metastatic colon cancer cells (Figure 7 D–F). After 24 hours of exposure, free 5-FU reduced cell viability from 90.62 ± 9.70% to 18.64 ± 5.96% across the concentration range (3.125–100 µg/mL). In contrast, cells treated with 5-FU-loaded $CaCO_3$ NPs displayed a more moderate decrease in viability, from 92.64 ± 2.10% at 3.125 µg/mL to 47.22 ± 2.11% at 100 µg/mL. At the 48-hour mark, free 5-FU showed a more pronounced reduction in cell viability, from 91.85 ± 8.94% to 25.07 ± 0.79%, while 5-FU-loaded $CaCO_3$ NPs led to a more controlled reduction, from 90.59 ± 3.64% to 38.13 ± 5.68%. After 72 hours, 5-FU-loaded $CaCO_3$ NPs demonstrated superior biocompatibility, maintaining higher cell viability (around 45.18%) than free 5-FU (around 12.2%) at the highest concentration. These findings underscore the therapeutic potential of $CaCO_3$ nanoparticles as an effective drug delivery system for 5-FU. The free 5-FU formulation showed a rapid and potent cytotoxic effect, reducing cell viability significantly across both cell lines within the first 24 hours. However, this potent cytotoxicity could potentially result in off-target effects and toxicity to healthy cells. In contrast, the 5-FU-loaded $CaCO_3$ NPs exhibited a more gradual release, reducing the immediate cytotoxicity and maintaining consistent levels of viability reduction over the 72-hour period. The sustained release of 5-FU from the nanoparticles offers a therapeutic advantage, providing prolonged drug exposure with potentially fewer side effects. The improved biocompatibility of the 5-FU-loaded $CaCO_3$ NPs suggests that higher doses can be delivered over time without the sharp toxicity peaks observed with free 5-FU. This controlled drug release enhances the therapeutic index of 5-FU, potentially allowing for higher cumulative doses with reduced side effects, ultimately improving the overall safety and efficacy of the treatment.

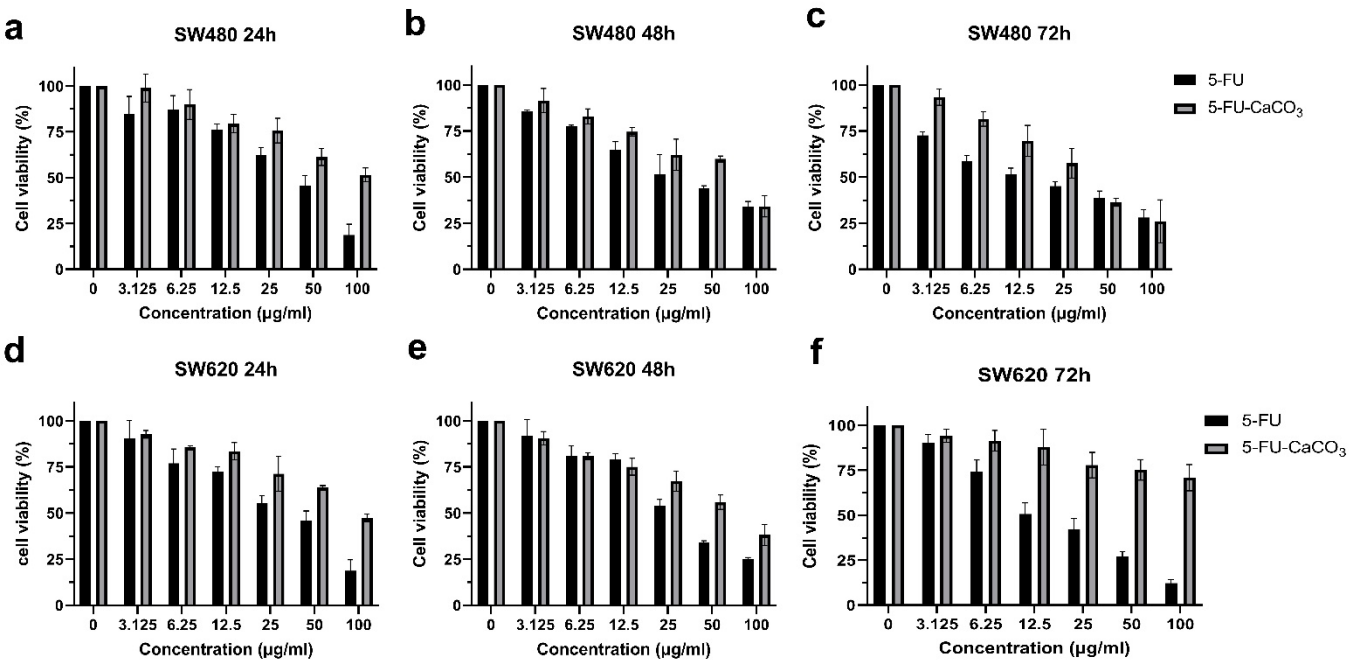


*Figure 7. Cell viability of SW480 (a–c) and SW620 (d–f) colon cancer cells treated with free 5-FU and 5-FU-loaded CaCO3 nanoparticles over 72 hours*

Supporting these findings, Figure 8 compares the biocompatibility and toxicity of $CaCO_3$ NPs with and without 5-FU in HS-27 human skin fibroblast cells. Toxicity was measured by the number of viable HS-27 cells determined by the MTT assay. There was no significant difference in cell numbers when cells were treated with $CaCO_3$ alone versus 5-FU loaded $CaCO_3$ NPs ($p > 0.05$), indicating the NPs alone do not significantly affect cell viability. In contrast, direct administration of 5-FU led to a drastic and significant decrease in cell numbers compared to treatments involving $CaCO_3$ NPs ($p < 0.0001$) and 5-FU-loaded $CaCO_3$ NPs ($p < 0.002$), respectively. This decrease highlights the potential of $CaCO_3$ NPs to reduce the cytotoxic effects of 5-FU when used as a delivery system, thus underscoring their potential to enhance the therapeutic index for chemotherapy drugs. Wang et al. also explored the concept of improving the therapeutic index of chemotherapy drugs using nanoparticle-based delivery systems [50].

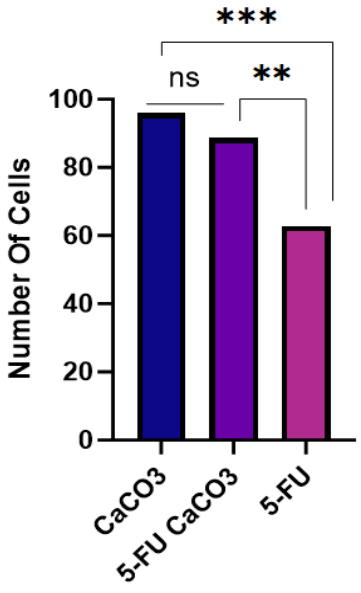


*Figure 8. Comparison of cell viability in HS-27 human skin fibroblast cells treated with CaCO3 NPs, 5-FU-loaded CaCO3 NPs, and Free 5-FU. Statistical analysis represents the difference between the corresponding CaCO3 NPs and free 5-FU with significance ($p < 0.0001$) and represents the difference between the 5-FU-loaded CaCO3 NPs and free 5-FU with significance less ($p < 0.002$) ($n = 3$).*

The IC50 values of 5-FU and 5-FU-$CaCO_3$ were assessed on the two colorectal cancer cell lines, SW480 and SW620, over 24, 48, and 72 hours. At the 24-hour mark, the IC50 of 5-FU-$CaCO_3$ was significantly higher than that of free 5-FU in both cell lines ($p < 0.001$), indicating a reduced cytotoxic effect upon nanoparticle loading. This trend persisted over time, with 5-FU-$CaCO_3$ showing consistently higher IC50 values than free 5-FU, particularly in SW620 cells, where the IC50 at 72 hours was significantly elevated ($p < 0.0001$). The consistent statistical significance across all time points ($p < 0.001$ or $p < 0.0001$) underscores the nanoparticle formulation's reduced potency and controlled-release characteristics.

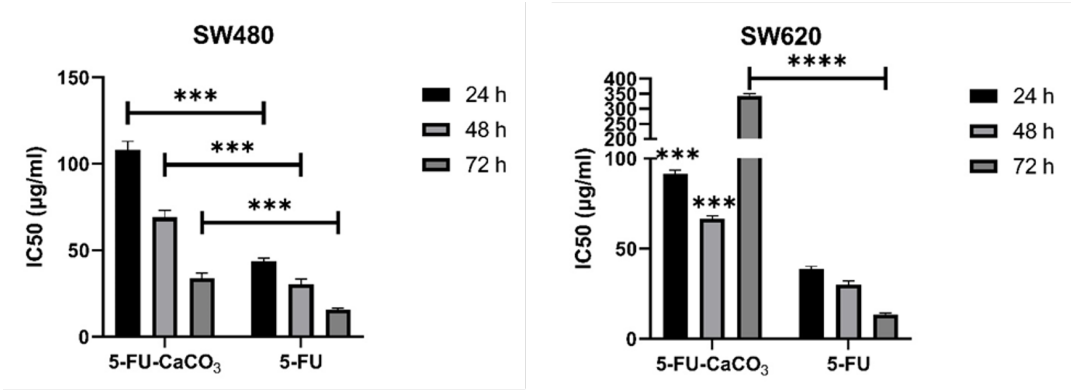


*Figure 9. IC50 values of 5-FU and 5-FU-loaded calcium carbonate nanoparticles (5-FU-$CaCO_3$) for colorectal cancer cell lines SW480 and SW620 at 24, 48, and 72 hours (n=3). ***p < 0.001, ****p < 0.0001*

These findings suggest that the $CaCO_3$-based delivery system moderates the immediate cytotoxicity of 5-FU, enhances its safety profile while maintains its therapeutic efficacy. This highlights the potential of $CaCO_3$ nanoparticles to improve the tolerability and effectiveness of chemotherapeutic agents in colorectal cancer treatment.

## Conclusion

This investigation demonstrates the successful encapsulation of 5-FU within aragonite $CaCO_3$ NPs derived from cockle shells. TEM revealed a notable increase in particle size following drug encapsulation, indicative of effective 5-FU loading. The interaction between 5-FU and $CaCO_3$ NPs was further confirmed by FTIR spectroscopy, supporting the hypothesis of a physically encapsulated drug-loading process. XRD analysis revealed changes in 5-FU crystallinity following encapsulation, while the crystalline structure of the $CaCO_3$ NPs remained unaffected. Percentage loading content, encapsulation efficiency, and drug-loading capacity were also assessed. Additionally, zeta potential analysis showed a reduction in surface charge after drug loading, which may influence particle stability and aggregation dynamics. The encapsulation of 5-FU in $CaCO_3$ NPs altered the drug release kinetics compared to free 5-FU, providing a more controlled-release profile. The Higuchi and Korsmeyer-Peppas models were best suited to describe this release, highlighting the potential of these NPs in sustained and targeted drug delivery applications. Biocompatibility assessments demonstrated that 5-FU-loaded $CaCO_3$ NPs exhibited negligible cytotoxicity toward non-neoplastic HS-27 fibroblast cells, underscoring the safety of the delivery system. In addition to non-neoplastic cells, cytotoxicity assays on SW480 (primary colon cancer) and SW620 (metastatic colon cancer) cell lines demonstrated that 5-FU-loaded $CaCO_3$ NPs induced a dose-dependent reduction in cell viability. However, compared to free 5-FU, the nanoparticle formulation exhibited a more controlled and sustained release, significantly reducing cytotoxic effects on cancer cells at all concentrations and time points. This supports the therapeutic potential of 5-FU-loaded $CaCO_3$ NPs in delivering targeted and safer cancer treatments with fewer side effects. These findings highlight the promising potential of $CaCO_3$ NPs as a drug delivery system for chemotherapy, offering a more controlled drug release and reducing systemic toxicity. The variation in results compared to previous studies highlights the complexity of nanoparticle drug delivery systems. It emphasizes the need for further research to optimize nanoparticle designs for specific therapeutic applications, particularly in cancer treatment.

Author Contributions:

Funding: This research was funded by the internal grant of Universiti Putra Malaysia, Malaysia, Geran Putra-IPM (GP-IPM/2020/9684800).

Acknowledgments: The authors gratefully acknowledge the vital assistance of the Universiti Putra Malaysia in providing technical support and electronic access to subscription databases.

Conflicts of Interest: The authors declare that they have no known competing financial interests or personal relationships that could have appeared to influence the work reported in this paper. The funders had no role in the study's design, data collection, analysis, interpretation, manuscript writing, or decision to publish the results.

Quote this article as Salem KMA, Ibrahim MA, Chan KM, Bakar ZA, Alitheen NB, Alsubbi M, Razis AFA, Ismail N, Synthesis and Characterization of Loaded 5-FU $CaCO_3$ Nanoparticles for Targeted Cancer Therapy, Precis. Nanomed. 2024, 7(4):1386-1405, https://doi.org/10.33218/001c.127799



## References

[1] M. Milczarek *et al.*, "In Vitro Evaluation of Sulforaphane and a Natural Analog as Potent Inducers of 5-Fluorouracil Anticancer Activity," *Molecules*, vol. 23, no. 11, p. 3040, Nov. 2018, doi: 10.3390/molecules23113040.

[2] N. Y. F. Elnehrawy, "IN VITRO STUDY OF POLYGONUM MINUS EXTRACT EFFECT ON SKIN CELLS HEALING CAPACITY."

[3] L. Giodini *et al.*, "NanocarrierNanocarriersclinical practice: a pharmacokinetic issue," *Nanomedicine Nanotechnol. Biol. Med.*, vol. 13, no. 2, pp. 583–599, Feb. 2017, doi: 10.1016/j.nano.2016.07.012.

[4] M. S. Taha, S. Padmakumar, A. Singh, and M. M. Amiji, "Critical quality attributes in the development of therapeutic nanomedicines toward clinical translation," *Drug Deliv. Transl. Res.*, vol. 10, no. 3, pp. 766–790, Jun. 2020, doi: 10.1007/s13346-020-00744-1.

[5] "Ghafar SLMA, et al. (2017). Synthesis and Characterization of Cockle Shell-Based Calcium Carbonate Aragonite Polymorph Nanoparticles with Surface Functionalization. Journal of Nanoparticles Volume 2017, Article ID 8196172, 12 pages.".

[6] S. T. Haque, M. M. Banaszak Holl, and E. H. Chowdhury, "Strategies to assemble therapeutic and imaging molecules into inorganic nanocarriernanocarriers*ater. Sci.*, vol. 16, no. 3, p. 220604, Sep. 2022, doi: 10.1007/s11706-022-0604-x.

[7] M. M. Mailafiya *et al.*, "Cytotoxicity Studies of Curcumin Loaded-cockle Shell-derived Calcium Carbonate Nanoparticles," *Nanosci. Nanotechnol.-Asia*, vol. 11, no. 1, pp. 35–41, Feb. 2021, doi: 10.2174/2210681209666191128155819.

[8] "Ibiyeye KM, et al. (2019). Ultrastructural Changes and Antitumor Effects of Doxorubicin/Thymoquinone Loaded CaCO3 Nanoparticles on Breast".

[9] M. Muhammad Mailafiya *et al.*, "Evaluation of In-Vitro Release Kinetic and Mechanisms of Curcumin Loaded-Cockle Shell-Derived Calcium Carbonate Nanoparticles," CHEMISTRY, preprint, Aug. 2019. doi: 10.20944/preprints201908.0254.v1.

[10] M. Oshi *et al.*, "Urine as a Source of Liquid Biopsy for Cancer," *Cancers*, vol. 13, no. 11, p. 2652, May 2021, doi: 10.3390/cancers13112652.

[11] M. Muhammad Mailafiya *et al.*, "Cockle Shell-Derived Calcium Carbonate (Aragonite) Nanoparticles: A Dynamite to Nanomedicine," *Appl. Sci.*, vol. 9, no. 14, p. 2897, Jul. 2019, doi: 10.3390/app9142897.

[12] S. L. Mohd Abd Ghafar, M. Z. Hussein, and Z. Abu Bakar Zakaria, "Synthesis and Characterization of Cockle Shell-Based Calcium Carbonate Aragonite Polymorph Nanoparticles with Surface Functionalization," *J. Nanoparticles*, vol. 2017, pp. 1–12, Jan. 2017, doi: 10.1155/2017/8196172.

[13] S. Chockalingam, G. Packirisamy, and R. Paulmurugan, "Editorial: Nanomaterials for targeted delivery of therapeutic and imaging agents," *Front. Cell Dev. Biol.*, vol. 10, p. 978690, Aug. 2022, doi: 10.3389/fcell.2022.978690.

[14] Q. Cheng, T. Wei, L. Farbiak, L. T. Johnson, S. A. Dilliard, and D. J. Siegwart, "Selective organ targeting (SORT) nanoparticles for tissue-specific mRNA delivery and CRISPR–Cas gene editing," *Nat. Nanotechnol.*, vol. 15, no. 4, pp. 313–320, Apr. 2020, doi: 10.1038/s41565-020-0669-6.

[15] Y. K. Sung and S. W. Kim, "Recent advances in polymeric drug delivery systems," *Biomater. Res.*, vol. 24, no. 1, p. 12, Dec. 2020, doi: 10.1186/s40824-020-00190-7.

[16] A. Gagliardi *et al.*, "Biodegradable Polymeric Nanoparticles for Drug Delivery to Solid Tumors," *Front. Pharmacol.*, vol. 12, p. 601626, Feb. 2021, doi: 10.3389/fphar.2021.601626.

[17] S. Mohd Abd Ghafar, M. Z. Hussein, Y. Rukayadi, and M. Z. Abu Bakar Zakaria, "Surface-functionalized cockle shell–based calcium carbonate aragonite polymorph as a drug nanocarrier*nanocarriernol. Sci. Appl.*, vol. Volume 10, pp. 79–94, May 2017, doi: 10.2147/NSA.S120868.

[18] K. M. Ibiyeye, A. B. Z. Zuki, N. Nurdin, and M. Ajat, "Combine Drug Delivery of Thymoquinone-Doxorubicin by Cockle Shellderived pH-sensitive Aragonite CaCO3 Nanoparticles," *Nanosci. Nanotechnol.-Asia*, vol. 10, no. 4, pp. 518–533, Aug. 2020, doi: 10.2174/2210681209666190508122540.

[19] V. Nayak, K. R. Singh, A. K. Singh, and R. P. Singh, "Potentialities of selenium nanoparticles in biomedical science," *New J. Chem.*, vol. 45, no. 6, pp. 2849–2878, 2021, doi: 10.1039/D0NJ05884J.

[20] B. L. Rivas, B. F. Urbano, and J. Sánchez, "Water-Soluble and Insoluble Polymers, Nanoparticles, Nanocomposites and Hybrids With Ability to Remove Hazardous Inorganic Pollutants in Water," *Front. Chem.*, vol. 6, p. 320, Jul. 2018, doi: 10.3389/fchem.2018.00320.

[21] L.-H. Liu and X.-Z. Zhang, "Carrier-free nanomedicines for cancer treatment," *Prog. Mater. Sci.*, vol. 125, p. 100919, Apr. 2022, doi: 10.1016/j.pmatsci.2021.100919.

[22] N. Anand, R. K. Kanwar, R. Sehgal, and J. R. Kanwar, "Antiparasitic and Immunomodulatory Potential of Oral Nanocapsules Encapsulated Lactoferrin Protein Against *Plasmodium Berghei*," *Nanomed.*, vol. 11, no. 1, pp. 47–62, Jan. 2016, doi: 10.2217/nnm.15.181.

[23] J. Kanwar, N. Anand, R. Sehgal, R. Kanwar, M. Dubey, and R. K. Vahishta, "Oral administration of encapsulated bovine lactoferrin protein nanocapsules against intracellular parasite Toxoplasma gondii," *Int. J. Nanomedicine*, p. 6355, Oct. 2015, doi: 10.2147/IJN.S85286.

[24] V. Popova, Y. Poletaeva, I. Pyshnaya, D. Pyshnyi, and E. Dmitrienko, "Designing pH-Dependent Systems Based on Nanoscale Calcium Carbonate for the Delivery of an Antitumor Drug," *Nanomaterials*, vol. 11, no. 11, p. 2794, Oct. 2021, doi: 10.3390/nano11112794.

[25] A. Danmaigoro, G. T. Selvarajah, M. H. M. Noor, R. Mahmud, and Md. Z. A. B. @ Zakaria, "Development of Cockleshell ( *Anadara granosa* ) Derived $CaCO_3$ Nanoparticle for Doxorubicin Delivery," *J. Comput. Theor. Nanosci.*, vol. 14, no. 10, pp. 5074–5086, Oct. 2017, doi: 10.1166/jctn.2017.6920.

[26] K. M. Ibiyeye and A. B. Z. Zuki, "Cockle Shell-Derived Aragonite CaCO3 Nanoparticles for Co-Delivery of Doxorubicin and Thymoquinone Eliminates Cancer Stem Cells," *Int. J. Mol. Sci.*, vol. 21, no. 5, p. 1900, Mar. 2020, doi: 10.3390/ijms21051900.

[27] L. Mamuroh and F. Nurhakim, "Health Education to Overcome Side Effects of Chemotherapy in Cancer Patients".

[28] "Ibiyeye et al. - 2020 - Cockle shell-derived aragonite calcium carbonate n.pdf."

[29] H. Ahmed *et al.*, "Modified methods of nanoparticles synthesis in pH-sensitive nano-carrienanocarriers for doxorubicin delivery on MCF-7 breast cancer cell line," *Int. J. Nanomedicine*, vol. Volume 14, pp. 3615–3627, May 2019, doi: 10.2147/IJN.S190830.

[30] "Hamidu A, et al. (2019). Modified methods of nanoparticles synthesis in pH-sensitive nano-carrienanocarriers for doxorubicin delivery on MCF-7 breast cancer cell line. International Journal of Nanomedicine 14, 3615– 3627".

[31] R. Kulsoom *et al.*, "Synthesis of calcium carbonate-quince bio-composite for programmed and on-demand drug release of paracetamol at target site: a green chemistry approach," *Polym. Bull.*, vol. 80, no. 6, pp. 6965–6988, Jun. 2023, doi: 10.1007/s00289-022-04400-1.

[32] P. Severino, C. F. Da Silva, L. N. Andrade, D. De Lima Oliveira, J. Campos, and E. B. Souto, "Alginate Nanoparticles for Drug Delivery and Targeting," *Curr. Pharm. Des.*, vol. 25, no. 11, pp. 1312–1334, Aug. 2019, doi: 10.2174/1381612825666190425163424.
[33] M. M. El-Hammadi, Á. V. Delgado, C. Melguizo, J. C. Prados, and J. L. Arias, "Folic acid-decorated and PEGylated PLGA nanoparticles for improving the antitumour activity of 5-fluorouracil," *Int. J. Pharm.*, vol. 516, no. 1–2, pp. 61–70, Jan. 2017, doi: 10.1016/j.ijpharm.2016.11.012.
[34] M. Ali *et al.*, "Anti-Arthritic and Anticancer Activities of Polyphenols: A Review of the Most Recent In Vitro Assays," *Life*, vol. 13, no. 2, p. 361, Jan. 2023, doi: 10.3390/life13020361.
[35] T. Liberato, D. S. Pessotti, I. Fukushima, E. S. Kitano, S. M. T. Serrano, and A. Zelanis, "Signatures of protein expression revealed by secretome analyses of cancer associated fibroblasts and melanoma cell lines," *J. Proteomics*, vol. 174, pp. 1–8, Mar. 2018, doi: 10.1016/j.jprot.2017.12.013.
[36] F. H. Zakarial Ansar *et al.*, "Pharmacokinetics and Biodistribution of Thymoquinone-loaded Nanostructured Lipid Carrier After Oral and Intravenous Administration into Rats," *Int. J. Nanomedicine*, vol. Volume 15, pp. 7703–7717, Oct. 2020, doi: 10.2147/IJN.S262395.
[37] P. Moulin and H. Roques, "Zeta potential measurement of calcium carbonate," *J. Colloid Interface Sci.*, vol. 261, no. 1, pp. 115–126, May 2003, doi: 10.1016/S0021-9797(03)00057-2.
[38] D. Mohan, Z. K. Teong, M. S. Sajab, N. H. N. Kamarudin, and H. Kaco, "Intact Fibrillated 3D-Printed Cellulose Macrofibrils/CaCO3 for Controlled Drug Delivery," *Polymers*, vol. 13, no. 12, p. 1912, Jun. 2021, doi: 10.3390/polym13121912.
[39] Z. A. Khan *et al.*, "A Comparative Study on Alvogyl and a Mixture of Black Seed Oil and Powder for Alveolar Osteitis: A Randomized Double-Blind Controlled Clinical Trial," *Int. J. Clin. Pract.*, vol. 2022, pp. 1–8, Feb. 2022, doi: 10.1155/2022/7756226.
[40] A. Kamba, M. Ismail, T. Ibrahim, and Z. Zakaria, "Biocompatibility of bio based calcium carbonate nanocrystals aragonite polymorph on NIH 3T3 fibroblast cell line," *Afr. J. Tradit. Complement. Altern. Med.*, vol. 11, no. 4, p. 31, Aug. 2014, doi: 10.4314/ajtcam.v11i4.5.
[41] L. Saidykhan, Y. Rukayadi, A. Umar Kura, L. S. Yazan, and M. Z. B. Abu Bakar, "Development of nanoantibiotic delivery system using cockle shell-derived aragonite nanoparticles for treatment of osteomyelitis," *Int. J. Nanomedicine*, p. 661, Feb. 2016, doi: 10.2147/IJN.S95885.
[42] A. Danmaigoro, G. T. Selvarajah, M. H. M. Noor, R. Mahmud, and Md. Z. A. B. @ Zakaria, "Development of Cockleshell ( *Anadara granosa* ) Derived $CaCO_3$ Nanoparticle for Doxorubicin Delivery," *J. Comput. Theor. Nanosci.*, vol. 14, no. 10, pp. 5074–5086, Oct. 2017, doi: 10.1166/jctn.2017.6920.
[43] D. Mohan, N. F. Khairullah, Y. P. How, M. S. Sajab, and H. Kaco, "3D Printed Laminated CaCO3-Nanocellulose Films as Controlled-Release 5-Fluorouracil," *Polymers*, vol. 12, no. 4, p. 986, Apr. 2020, doi: 10.3390/polym12040986.
[44] "Islam et al. - 2012 - Facile Synthesis of Calcium Carbonate Nanoparticle.pdf."
[45] K. M. Ibiyeye, S. B. Idris, and A. B. Z. Zuki, "Cockle shell-derived aragonite calcium carbonate nanoparticle for targeting cancer and breast cancer stem cells," *Cancer Nanotechnol.*, vol. 11, no. 1, p. 10, Dec. 2020, doi: 10.1186/s12645-020-00067-3.
[46] T. M. Kiio and S. Park, "Physical properties of nanoparticles do matter," *J. Pharm. Investig.*, vol. 51, no. 1, pp. 35–51, Jan. 2021, doi: 10.1007/s40005-020-00504-w.
[47] A. M. Hersh, S. Alomari, and B. M. Tyler, "Crossing the Blood-Brain Barrier: Advances in Nanoparticle Technology for Drug Delivery in Neuro-Oncology," *Int. J. Mol. Sci.*, vol. 23, no. 8, p. 4153, Apr. 2022, doi: 10.3390/ijms23084153.
[48] D. Chenthamara *et al.*, "Therapeutic efficacy of nanoparticles and routes of administration," *Biomater. Res.*, vol. 23, no. 1, p. 20, Dec. 2019, doi: 10.1186/s40824-019-0166-x.
[49] J. Fu, Y. Xu, Y. Yang, Y. Liu, L. Ma, and Y. Zhang, "Aspirin suppresses chemoresistance and enhances antitumor activity of 5-Fu in 5-Fu-resistant colorectal cancer by abolishing 5-Fu-induced NF-κB activation," *Sci. Rep.*, vol. 9, no. 1, p. 16937, Nov. 2019, doi: 10.1038/s41598-019-53276-1.
[50] P. Wang, F. Tong, J. Luo, Z. Li, J. Wei, and Y. Liu, "Fucoidan-Mediated Anisotropic Calcium Carbonate Nanorods of pH-Responsive Drug Release for Antitumor Therapy," *Front. Bioeng. Biotechnol.*, vol. 10, p. 845821, Apr. 2022, doi: 10.3389/fbioe.2022.845821.

[51] M. S. Ghaji, Z. A. B. Zakaria, I. Shameha A. R., M. H. M. Noor, and H. Hazilawati, "Novel Synthesis of Nanoparticles from Cockle Shells via Mechanical Method for Cytarabine Drug Release," *J. Comput. Theor. Nanosci.*, vol. 15, no. 4, pp. 1128–1136, Apr. 2018, doi: 10.1166/jctn.2018.6943.

[52] A. Danmaigoro, G. T. Selvarajah, M. H. Mohd Noor, R. Mahmud, and M. Z. Abu Bakar, "Toxicity and Safety Evaluation of Doxorubicin-Loaded Cockleshell-Derived Calcium Carbonate Nanoparticle in Dogs," *Adv. Pharmacol. Sci.*, vol. 2018, pp. 1–20, Jun. 2018, doi: 10.1155/2018/4848602.

[53] A. Z. Jaji *et al.*, "Safety assessments of subcutaneous doses of aragonite calcium carbonate nanocrystals in rats," *J. Nanoparticle Res.*, vol. 19, no. 5, p. 175, May 2017, doi: 10.1007/s11051-017-3849-z.

[54] P. Severino, C. F. Da Silva, L. N. Andrade, D. De Lima Oliveira, J. Campos, and E. B. Souto, "Alginate Nanoparticles for Drug Delivery and Targeting," *Curr. Pharm. Des.*, vol. 25, no. 11, pp. 1312–1334, Aug. 2019, doi: 10.2174/1381612825666190425163424.

[55] "Jungblut and Eychmüller - 2019 - Modeling nanoparticle aggregation.pdf."

[56] S. Jungblut and A. Eychmüller, "Modeling nanoparticle aggregation," in *Chemical Modelling*, vol. 15, M. Springborg and J.-O. Joswig, Eds., Cambridge: Royal Society of Chemistry, 2019, pp. 1–27. doi: 10.1039/9781788015868-00001.

[57] F. R. Bastos, D. Soares Da Costa, R. L. Reis, N. M. Alves, I. Pashkuleva, and R. R. Costa, "Layer-by-layer coated calcium carbonate nanoparticles for targeting breast cancer cells," *Biomater. Adv.*, vol. 153, p. 213563, Oct. 2023, doi: 10.1016/j.bioadv.2023.213563.

[58] R. Gupta, "A Thesis Presented to The Academic Faculty".

[59] A. Shafiu Kamba, M. Ismail, T. A. Tengku Ibrahim, and Z. A. B. Zakaria, "A pH-Sensitive, Biobased Calcium Carbonate Aragonite Nanocrystal as a Novel Anticancer Delivery System," *BioMed Res. Int.*, vol. 2013, pp. 1–10, 2013, doi: 10.1155/2013/587451.

[60] P. Mukherjee and S. Mani, "Methodologies to decipher the cell secretome," *Biochim. Biophys. Acta BBA - Proteins Proteomics*, vol. 1834, no. 11, pp. 2226–2232, Nov. 2013, doi: 10.1016/j.bbapap.2013.01.022.

[61] S. Maleki Dizaj, M. Barzegar-Jalali, M. H. Zarrintan, K. Adibkia, and F. Lotfipour, "Calcium carbonate nanoparticles as cancer drug delivery system," *Expert Opin. Drug Deliv.*, vol. 12, no. 10, pp. 1649–1660, Oct. 2015, doi: 10.1517/17425247.2015.1049530.

[62] H. Zhao *et al.*, "In vitro additive antitumor effects of dimethoxycurcumin and 5-fluorouracil in colon cancer cells," *Cancer Med.*, vol. 6, no. 7, pp. 1698–1706, Jul. 2017, doi: 10.1002/cam4.1114.

[63] L. M. Johnson *et al.*, "Characterization of a Reservoir-Style Implant for Sustained Release of Tenofovir Alafenamide (TAF) for HIV Pre-Exposure Prophylaxis (PrEP)," *Pharmaceutics*, vol. 11, no. 7, p. 315, Jul. 2019, doi: 10.3390/pharmaceutics11070315.

[64] S. H. Lee *et al.*, "Deep Tumor Penetration of Drug-Loaded Nanoparticles by Click Reaction-Assisted Immune Cell Targeting Strategy," *J. Am. Chem. Soc.*, vol. 141, no. 35, pp. 13829–13840, Sep. 2019, doi: 10.1021/jacs.9b04621.

[65] A. Shafiu Kamba, M. Ismail, T. A. Tengku Ibrahim, and Z. A. B. Zakaria, "A pH-Sensitive, Biobased Calcium Carbonate Aragonite Nanocrystal as a Novel Anticancer Delivery System," *BioMed Res. Int.*, vol. 2013, pp. 1–10, 2013, doi: 10.1155/2013/587451.

[66] "Fu W, et al. (2017). In vitro evaluation of a novel pH sensitive drug delivery system based cockle shell derived aragonite nanoparticles against osteosarcoma. J Exp Nanosci. 12(1), 166–1".

[67] J.-L. Wu, C.-Q. Wang, R.-X. Zhuo, and S.-X. Cheng, "Multi-drug delivery system based on alginate/calcium carbonate hybrid nanoparticles for combination chemotherapy," *Colloids Surf. B Biointerfaces*, vol. 123, pp. 498–505, Nov. 2014, doi: 10.1016/j.colsurfb.2014.09.047.

[68] C. Meindl, T. Kueznik, M. Bösch, E. Roblegg, and E. Fröhlich, "Intracellular calcium levels as screening tool for nanoparticle toxicity," *J. Appl. Toxicol.*, vol. 35, no. 10, pp. 1150–1159, Oct. 2015, doi: 10.1002/jat.3160.

[69] S. F. Lam, K. W. Bishop, R. Mintz, L. Fang, and S. Achilefu, "Calcium carbonate nanoparticles stimulate cancer cell reprogramming to suppress tumor growth and invasion in an organ-on-a-chip system," *Sci. Rep.*, vol. 11, no. 1, p. 9246, Apr. 2021, doi: 10.1038/s41598-021-88687-6.